Journal of Photochemistry & Photobiology, A: Chemistry 422 (2022) 113571

Contents lists available at ScienceDirect

Journal of Photochemistry & Photobiology, A: Chemistry

journal homepage: www.elsevier.com/locate/jphotochem

Photopolymerization of ionic liquids in flexible microporous aramids for ion conductive solid polyelectrolytes

M. Trigo López [a], J.A. Reglero Ruiz [a], J.L. Pablos [b,*], D.E. Ciurduc [c], T. Corrales [b,*], F.C. García [a], J.M. García [a]

[a] Departamento de Química, Facultad de Ciencias, Universidad de Burgos, Plaza de Misael Bañuelos s/n, 09001 Burgos, Spain
[b] Grupo de Fotoquímica de Polímeros, Instituto de Ciencia y Tecnología de Polímeros, Consejo Superior de Investigaciones Científicas, ICTP-CSIC, Juan de la Cierva 3, 28006 Madrid, Spain
[c] Electrochemical Processes Unit, IMDEA Energy, Av. Ramón de La Sagra, 3, 28935 Móstoles, Spain

ARTICLE INFO

Keywords:
Microporous aramid
Flexible solid electrolytes
Photopolymerizable ionic liquids

ABSTRACT

This work presents the preparation of novel solid polymer electrolytes based on flexible microporous aramids filled with photopolymerized ionic liquids and lithium salt. The materials combined a high ionic conductivity with the mechanical and thermal characteristics of the aramids, including also good flexibility and handleability. First, a simple casting process was followed to obtain microporous aramids with an interconnected channel morphology. In a second step, this channel structure was filled with a solution of non-commercial photopolymerizable ionic liquid, commercial ionic liquids and the lithium salt, followed by UV irradiation to obtain the conducting aramids. Ionic conductivity of the materials was studied at 25 °C, and also in the temperature range between −50 to 90 °C, together with SEM analyses of the filled porous structure and thermal properties, to fully characterize the photopolymerization process of the ionic liquids inside the porous structure. The materials showed high ionic conductivity values together with excellent thermal and mechanical properties, indicating their viability as flexible and thermally stable solid electrolytes.

1. Introduction

Solid-state polymer electrolytes for application in lithium batteries has become one of the most important research topics in the last decade, which is driven by the need to enhance their safety together with the development of flexible electrolytes with good electrochemical stability and high conductivity values [1,2]. Mainly, the fabrication of solid gel polymer electrolytes uses polyethylene oxide (PEO) to dissolve lithium salts [3], and following this research line, different approaches have been carried out to improve the ability to transport lithium ions, such as the addition of ceramic fillers [4] or carbon nanotubes [5]. One of the most promising researches to improve the performance of lithium metal polymer batteries is the addition of ionic liquids (ILs) [6,7]. In this sense, ILs can be employed as plasticizers, lowering the glass transition temperature of PEO improving the ionic mobility and, therefore, their ionic conductivity [8].

For this reason, ternary systems (polymer-lithium salt-IL) have been investigated, (in which PEO acts as host polymer), in terms of the different interaction mechanisms between all the components [9,10]. Among all the ILs investigated, imidazolium-based ILs present good miscibility with PEO, and ionic conductivity can be controlled with the quantity of IL [11]. However, there is a major disadvantage in the use of PEO, concerning its insufficient ionic conductivity derived from the crystallinity of the ethylene oxide sequences, which can restrain the ionic transition due to the stiff structure, especially at low temperature [12]. Then, different alternatives are currently being explored, employing other amorphous polymers such as poly(methyl methacrylate) or poly(methyl acrylate) [13].

Currently, the main research line to obtain highly efficient lithium batteries is focused in the design of solid electrolytes with electrochemical characteristics comparable to those of liquid ones, the so called solid-gel electrolytes. These materials must combine high ionic diffusivity (and hence high ionic conductivity) and dimensional stability. In this field, one of the best candidates are polymer ionic liquids (PILs), in which ILs are chemically linked through different polymerization mechanisms [14]. Although different ILs have been employed to enhance ionic conductivity [7], imidazolium-based ILs have emerged as the ideal candidates to obtain highly efficient ion gel electrolytes

* Corresponding authors.
E-mail addresses: jlpablos@ictp.csic.es (J.L. Pablos), tcorrales@ictp.csic.es (T. Corrales).

https://doi.org/10.1016/j.jphotochem.2021.113571
Received 26 May 2021; Received in revised form 22 September 2021; Accepted 25 September 2021
Available online 4 October 2021

[15,16], related to their high thermal stability which is partly assigned to the aromatic nature of the ring as well as intermolecular hydrogen-bonding [17]. Moreover, imidazolium-based ionic liquids show high ionic conductivities reaching values of 10^{-2} S/cm in addition to a sufficiently high value of electrochemical window for these compounds of about 4 V [18], that allows for a broad application range for solid polymer electrolytes device fabrication [19].

The literature regarding PILs is extensive [20]. For example, Washiro *et al.* [21] employed imidaziolium-based ionic liquids polymers with different hydrocarbon chain lengths, and Ahiara *et al.* [22] used PEO copolymers to prepare flexible polymer films to be used as solid electrolytes, but the obtained materials presented a low glass transition temperature, thus limiting drastically their applicability. Appetecchi *et al.*, reported the electrochemical properties of ternary polymer electrolytes for lithium batteries based on a novel poly(diallyldimethylammonium) bis(trifluoromethanesulfonyl)imide, incorporating pyrrolidinium-based polymeric ionic liquids [23]. Also, our group has developed ion gel electrolytes using photopolymerizable ILs, such as 1-(2-methacryloyloxy)ethyl-3-butylimidazolium bis(trifluoromethane sulfonyl) imide (IMMA), and a mixture of 1-ethyl-3-methylimidazolium bis(fluorosulfonyl)imide (EMIFSI) or 1-butyl-1-methylpyrrolidinium bis (fluorosulfonyl)imide (BMPFSI) and bis(trifluoromethane)sulfonimide lithium salt (LiTFSI), presenting high ionic conductivity at RT ($\approx 10^{-2}$ S/cm) and good thermal stability up to 200 °C [24]. Bearing all these ideas in mind, it is clear that there is a need to obtain new materials to be used as solid-gel electrolytes, combining different characteristics, such as high thermal resistance, high ionic conductivity in a wide range of temperatures, flexibility and mechanical stability.

In parallel, our group has developed an easy method to obtain microporous aramids, based in the use of ILs to generate controlled porosity. These materials present exceptional mechanical and thermal stability (up to 350 °C), combined with low density (around 0.2 g/cm^3, a reduction of 6 times respect to dense aramid) and excellent flexibility and handleability [25]. These materials can be employed as a polymeric scaffold in which polymerizable ionic liquids and lithium salts can be introduced, taking advantage of the surface porosity of the aramids. In a second phase, polymerization can take place inside the porous structure, obtaining a solid gel electrolyte with high ionic conductivity and excellent mechanical and thermal properties. The literature already shows several works in which porous polymers are employed as solid gel electrolytes in lithium ion batteries [26], mainly based in porous poly (vinylidene fluoride) (PVDF) [27,28], lithium poly[4-styrenesulfonyl (phenylsulfonyl)imide] [29] or poly(diallyldimethylammonium) bis (trifluoromethanesulfonyl)imide [30]. However, the basis of our approach is completely different, microporous aramids are employed as solid polymeric supports in which the photopolymerization of the IL is carried out inside the porous structure previously prepared. In this way, ion conductivity is also enhanced through physical methods, due to the specific porous morphology, in which their interconnected microchannels would allow great ion mobility between the electrodes.

Then, the main objective of this work is to develop new solid-gel polymeric materials based on photopolymerisation of ILs inside microporous aramids, having optimum properties to be used as highly ionic conductive solid electrolyte. In our approach, the porous aramid acts as a polymeric support and the ionic conductivity is related exclusively to the system lithium salts/ILs, which is introduced filling the interconnected porous structure of the aramid, and photopolymerized afterwards. This new material combines the excellent thermal and mechanical stability, good handleability and flexibility of the aramids, together with the excellent ionic conductivity provided by the ionic liquid, opening an interesting research field in which these materials could be used as solid polymeric electrolytes in Li-ion batteries.

2. Experimental

2.1. Materials

All materials, reactants and solvents were used as received. Commercial poly(*m*-phenylene isophthalamide) (MPIA), aramid fiber Twaron® (nonwoven regular staple fiber of average length 6.4 mm, 4.94 cN/dtex, $\rho \approx 1.38$ g/cm^3 and $T_m > 400$ °C), was used. Two different ionic liquids were employed: 1-ethyl-3-methylimidazolium bromide (IL) (≥97 %), purchased from Sigma-Aldrich, and 1-ethyl-3-methylimidazolium bis(trifluoromethane)sulfonamide (EMIM TFSI, 99.5 %) purchased from Solvionic. Ethyleneglycol dimethacrylate (EGDM, 98 %), crosslinker bis(trifluoromethane) sulfonamide lithium salt (LiTFSI, 99.95 %), and Irgacure 659 (photointiator, 98 %) were purchased from Sigma-Aldrich.

2-bromoethanol (95 %), triethylamine (>99 %), methacryloyl chloride (97 %), 1-butylimidazole (98 %), *N,N*-dimethylacetamide (DMAc, > 99 %) and dichloromethane (DCM, 99.99 %) were employed, all of them purchased from Sigma-Aldrich. Hydroquinone (99.5 %) was purchased from Panreac, and finally milliQ water and hexane (99.8 %), purchased from Scharlau, were used.

2.2. Characterization and procedures

SEM micrographs were taken using a Scanning Electronic Microscope JEOL JSM-6460LV. Aramid films were frozen in liquid nitrogen, fractured and gold coated in vacuum to assure the electrical conductivity of the materials. For filled materials, SEM pictures were taken without gold coating. It has been observed, that the conditions of high vacuum of SEM analysis procedure did not affect to the liquid or polymerized phase of aramid discs. Porous structure was characterized by determining the average bubble radius $\overline{R}$ and average cell density from SEM images was measured using ImageJ® software and consisted of counting the number of bubbles in each image n_i and its radius R_i [31]. The average radius was calculated using Eq. (1), where N represents the bubble count.

$$\overline{R} = \frac{\sum_{i=1}^{N} n_i R_i}{\sum_{i=1}^{N} n_i} \tag{1}$$

Three different SEM images were analyzed from each material, and the data was averaged. The estimation of the cell density N_c was calculated using the Kumar's approximation, as shown in Eq. (2), where n is the number of cells in the image and A is the area of the image. The description of the calculation method can be found in our previous work [32]

$$N_c = \left(\frac{n}{A}\right)^{3/2} \tag{2}$$

Density was determined from the dimensions and weight of the samples, determining the thickness by directly using a digital micrometer.

The thermogravimetric analysis data were recorded on a TA Instrument Q50 TGA analyzer. TGA tests were performed under O_2 (synthetic air) atmosphere using the next procedure: first, samples were heated from RT to 100 °C at 10 °C/min, and then kept during 10 min to eliminate the moisture content. Then, samples were heated up to 800 °C at 10 °C/min.

Differential Scanning Calorimetry (DSC) tests were performed in a DSC Q200 TA Instruments to evaluate the thermal transitions of the materials. First, after 5 min of stabilization at 30 °C, samples were heated to 250 °C at 15 °C/min. Then, the samples were stabilized for 5 min at 250 °C and cooled down to −80 °C to erase the thermal history. Then, a second heating ramp up to 250 °C was carried out at 15 °C/min. Finally, samples were cooled down to RT at 15 °C/min. All tests were performed under N_2 atmosphere (flow rate 50 ml/min), with a mass

sample of approximately 15 mg.

Ionic conductivity of the membranes was determined at RT and also in a temperature range from −50 °C to 90 °C. The ionic conductivity behavior of the electrolytes was determined in a NOVOCONTROL GmbH Concept 40 broadband dielectric spectrometer in the frequency range between 1 and 10^7 Hz. Disk films of dimensions of 16 mm diameter and around 200 μm thickness were inserted between two gold-plated flat electrodes, the samples were cooled down to − 50 °C. Then, a frequency sweep was carried out every 10 °C heating up to 90 °C.

The photopolymerization reactions were carried out in a Biolink™ BLX-365 type Bio-link apparatus (Vilbert Lourmat™) by irradiation with UV light (365 nm) for 55 min.

2.3. Film preparation

Firstly, the synthesis of the ionic liquid used in the photopolymerizable formulation is described [15,23], (section 2.3.1). Secondly, the fabrication of the microporous aramids is detailed (section 2.3.2). To conclude, the filling and photopolymerization process of the formulation inside the porous structure of the aramids is described (section 2.3.3).

2.3.1. Synthesis of the monomer 1-(2-methacryloyloxy)ethyl-3-butylimidazolium bis(trifluoromethane sulfonyl)imide (ILQ)

1-(2-methacryloyloxy)ethyl-3-butylimidazolium bis(trifluoromethane sulfonyl)imide monomer was employed as the imidazolium-based polymerizable ionic liquid. We will denote this monomer as (ILQ), to clearly differentiate it from the ionic liquid (1-ethyl-3-methylimidazolium bromide, named as IL) employed to obtain the porous structure in the aramids. The synthesis process was carried out in three steps. First, the monomer 2-bromoethyl methacrylate (L_1) was synthetized. Secondly, the monomer 1-(2-methacryloyloxy)ethyl-3-butylimidazolium bromide (L_2) was obtained to finally prepare in the last step the 1-(2-methacryloyloxy)ethyl-3-butylimidazolium bis(trifluoromethane sulfonyl)imide (ILQ). The synthesis procedure and characterization results of each reaction product can be found in detail in one of our previous works [15].

2.3.2. Preparation of microporous aramid films

The preparation of microporous aramid films firstly involves obtaining dense aramid films (pure aramid films filled with IL). Aramid fibers were dissolved in hot DMAc (60 °C), containing 2 % wt. of LiCl respect to the volume of DMAc to improve the solubility of aramid fiber in DMAc. To obtain the microporous structure, 1-ethyl-3-methylimidazolium bromide (IL) was added to the solution in a proportion of 10/90 wt (MPIA:LI) and stirred for 3 h. Then, the solution was poured into a glass plate of 20 × 20 cm and placed inside an oven at 85 °C during at least 24 h, until the complete evaporation of the solvent. Dense films were termed as 10ARA/90IL.

Microporous aramid films were fabricated by simply washing dense films in distilled water at 80 °C for 4 h replacing the distilled water three times to remove the IL and at the same time, the possible traces of remaining solvent. Porous films after IL removal were denoted as (10ARA/90IL)-R. It is important to remark that the proportion of the IL was 10/90 wt (MPIA:LI) to assure the presence of an interconnected micro-channel porous structure after IL removal. Lower proportions of IL were already tested in a previous work, leading to closed-cell porosity that could limit the efficiency of the filling process [25]. Using this methodology, porous materials of around 100 cm^2 were obtained.

At least 5 discs of 16 mm diameter were punched from the porous film-shaped material to proceed afterwards to the filling and polymerization of the formulation including ILQ inside the porous structure. Fig. S1 shows a photograph of aramid discs (pure aramid films without IL, dense aramid film filled with IL and porous aramid film after IL removal). It is observed that discs after IL removal present a high degree of opacity (Fig. S1c) evidencing the generation of a porous structure in which light is diffracted and reducing drastically the transparency observed in pure and dense aramids (Fig. S1a and b). Thicknesses of the discs were around 200 μm.

Average density values were calculated from the individual measurement of at least three discs of each film (pure, dense and porous). Although many different works present the characterization of imidazolium-based ionic liquids [33], the literature does not indicate the density of this specific IL. However, we can estimate the density of the IL using the mixture's law for two-phase materials, obtaining a density value of the IL around 1.19 g/cm^3, lying in the range of typical density value reported for similar imidazolium-based ILs [34]. Density of porous aramids was decreased to 0.17 ± 0.04 g/cm^3, thus a reduction by a factor of approximately 8 respect to pure MPIA.

2.3.3. Photopolymerization process

Table 1 shows the composition of the solution employed, in which ILQ corresponds to the synthesized polymerizable ILs, EMIM TFSI the commercial IL, LiTFSI the lithium salt and EGDM was included as crosslinker. All the compounds listed in Table 1 were transferred to a glass vial, degassed by nitrogen bubbling and sonicated for 10 min. Then, 1 ml of the solution was injected in a circular PTFE mold, and a porous aramid disc of 12 mm diameter was immersed into the prepared solution and maintained in dark and under an oxygen-free atmosphere for 72 h to facilitate a homogenous filling along the disc.

After that, the filled aramid was taken out of the solution and then drained to remove the residual solution, and photopolymerized under nitrogen atmosphere, by irradiation with UV light (365 nm) at RT for 55 min. Finally, the materials were dried in vacuum at 50 °C for 3 days to obtain the flexible solid electrolyte. These discs were named as ARA_{IMID}.

In a similar way, two supplementary materials were prepared, one of them polymerized only with the mixture of polymerizable ionic liquid, crosslinker and photoinitiator, without using EMIM TFSI and LiTFSI (named as $ARA_{ILQ\text{-}pol}$) and a second one, only filled (not polymerized) exclusively with the ionic liquid ILQ (named as $ARA_{ILQ\text{-}fil}$). It has to be pointed out that in the conditions used in this work, and during the time scale of analysis, it was no observed any visible evidence of leaking for the porous aramid membranes swollen with ionic liquid or photocurable composition. The comparative behavior of both materials will be analyzed to characterize the polymerization of the ionic liquid inside the porous structure. Density of the materials obtained was 1.16 g/cm^3 for $ARA_{ILQ\text{-}fil}$ samples, 1.42 g/cm^3 for $ARA_{ILQ\text{-}pol}$ samples and 1.35 g/cm^3 in the case of ARA_{IMID} samples. Comparing these values with the density of the initial porous material ($\rho \approx 0.17$ g/cm^3), it is confirmed that, in all the cases, the solution has effectively penetrated inside the porous channel structure. The films prepared, their composition and nomenclature are summarized in Table 2.

3. Results and discussion

The results section is divided in four subsections. In section 3.1., the microporous structure of aramids after the IL removal is analyzed through SEM images and the morphological parameters are determined. The filling and photopolymerization process of the ionic liquid ILQ

Table 1
Composition of the photopolymerizable formulation used in the porous aramid swelling process.

Material	% wt.
ILQ	24.54
EMIM TFSI	55.26
LiTFSI	20.20
EGDM*	1.00
Photoinitiator*	1.50

* EGDM data is given in % mol with respect to % mol of comonomers and photoinitiator data is given in % wt. with respect to total weight.

Table 2
Composition and nomenclature of the films.

Film	Composition							Characteristics
	MPIA	IL	ILQ	EMIM TFSI	LiTFSI	EGDM	Photoi	
10ARA/90IL	✓	✓	–	–	–	–	–	Dense (Aramid + IL)
(10ARA/90IL-R	✓	–	–	–	–	–	–	Porous (After IL removal)
ARA_{IMID}	✓	–	✓	✓	✓	✓	✓	Filled with formulation (Table 1) and polymerized
$ARA_{ILQ\text{-}fil}$	✓	–	✓	–	–	–	–	Filled with ILQ and non-polymerized
$ARA_{ILQ\text{-}pol}$	✓	–	✓	–	–	✓	✓	Filled with ILQ and polymerized

inside the porous structure is described in section 3.2., paying attention to the TGA, SEM and weight determination results of $ARA_{ILQ\text{-}pol}$ and $ARA_{ILQ\text{-}fil}$, to characterize the polymerization process. Finally, in section 3.3 the ionic conductivity values of the materials are presented.

3.1. Porous structure

A homogeneous microporous structure was observed in the aramid discs after the IL removal. SEM observations were taken in the cross section and also in the surface of the materials, Fig. 1.

Cross section SEM images of 10ARA/90IL-R discs show a homogeneous open-cell microporous structure with an average pore diameter $\overline{R}$ around 700 nm and cell sizes of $1.5 \cdot 10^{13}$ cells/cm^3, Fig. 1a and b. However, we must remark that the determination of the morphological parameters can be difficult in open-cell structures or in these morphologies based on open interconnected micro channels.

Fig. 1c and d present the SEM images of the surface of the porous aramids. In this case, a regular distribution of closed pores between 1 and 2 μm of diameter is observed. It is important to remark that this surface porosity has been also observed in similar porous materials obtained using ILs, such as PMMA [35]. This porosity very likely promotes the filling of the materials with the ionic liquid solution.

3.2. Study of photopolymerization process

Radical photopolymerizable formulation including the ionic liquids was undertaken by irradiating the material embedded in the solution with UV light (365 nm) at RT. Polymerization time was fixed to 55 min [15,23]. This polymerization time assured that UV light penetrated inside the whole thickness of the film (≈200 μm), and also guaranteed that the opacity of the materials due to the porosity did not affect to the polymerization efficiency.

The characterization of the filled and polymerized aramids was carried out through different techniques. First, thermal stability of the aramids was analyzed by standard TGA measurements, in order to evaluate the different thermal behavior of filled and polymerized discs. TGA curves of all the materials prepared are presented in Fig. S2. The analysis of the onset degradation temperatures, Table 3, shows that the removal of IL is evidenced, by comparing the onset temperatures of 10ARA/90IL and 10ARA/90IL-R (279 and 452 °C, respectively). Also, it can be observed an appreciable difference in the onset values from $ARA_{ILQ\text{-}fil}$ (348 °C) and $ARA_{ILQ\text{-}pol}$ (376 °C). This could indicate also the formation of a crosslinked structure in the $ARA_{ILQ\text{-}pol}$ derived of the polymerization process of the ILQ. It is also noticed that in terms of thermal degradation, ARA_{IMID} and $ARA_{ILQ\text{-}pol}$ show the same behavior

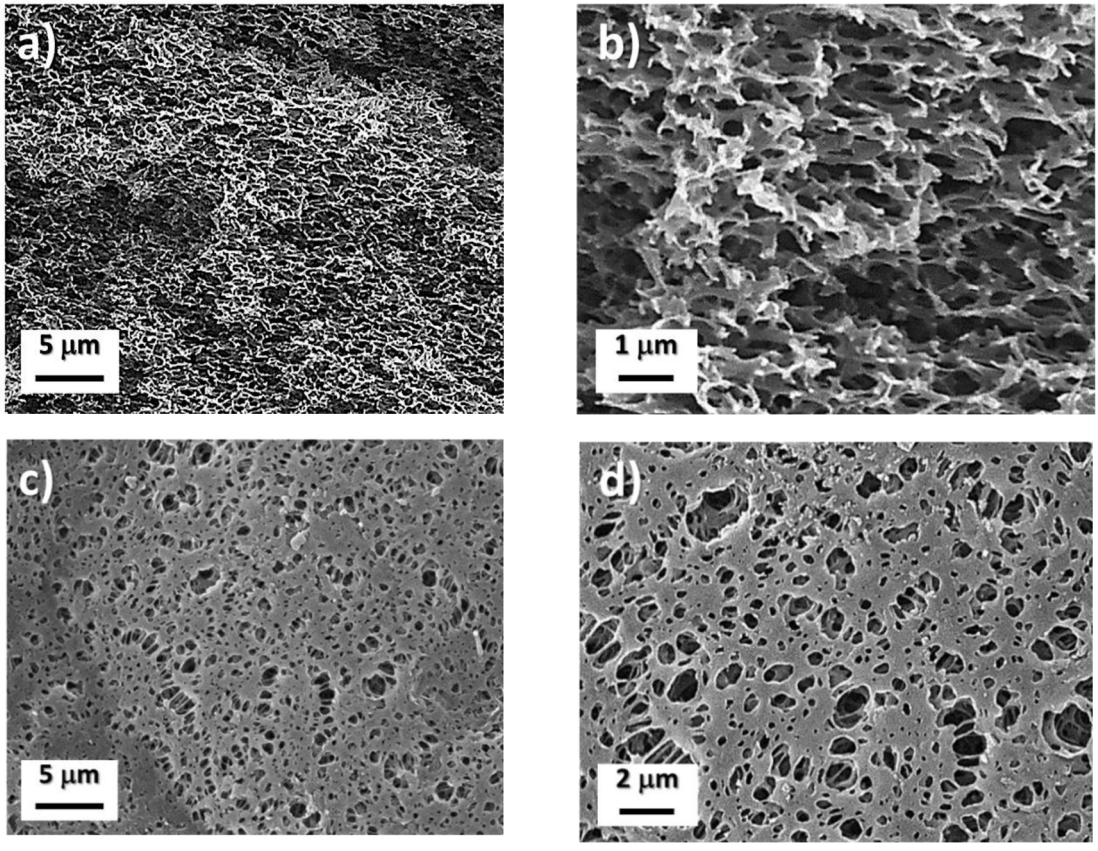

Fig. 1. SEM images of the 10ARA/90IL-R discs: a) and b) cross section; c) and d) surface.

Table 3
Thermal properties of aramids in oxidant atmosphere (synthetic air) (*extrapolated onset temperature* is defined as the temperature at which the decomposition of the material begins).

Film	Extrapolated onset temperatura (°C)
10ARA/90IL	279
10ARA/90IL-R	452
ARA_{IMID}	381
$ARA_{ILQ\text{-}fil}$	348
$ARA_{ILQ\text{-}pol}$	376

(onset temperatures are 381 and 376 °C, respectively) as consequence of the polymerization of ILQ, since all the imidazolium ILs containing [TFSI] anion are the most stable ILs [36]. Also, the influence of the anion in the imidazolium ring of the ionic liquid is evidenced comparing the onset temperatures of 10ARA/90IL (279 °C) which contains 1-ethyl-3-methylimidazolium bromide, and $ARA_{ILQ\text{-}fil}$ (348 °C), containing 1-(2-methacryloyloxy)ethyl-3-butylimidazolium bis(trifluoromethane sulfonyl)imide. In ARA_{IMID}, $ARA_{ILQ\text{-}fil}$ and $ARA_{ILQ\text{-}pol}$ materials, the presence of the ILQ is detected, and onset temperature values are in the same range (between 350 °C and 380 °C), corresponding to degradation of the side groups (such as imidazolium cations) of the IL together with the degradation of the main chain of the aramid matrix.

By DSC analysis, the glass transition of the polymerized ILQ embedded in the porous aramid $ARA_{ILQ\text{-}pol}$ is detected around −20 °C. This low glass transition value of the polymerized ionic liquid makes possible the ion transport inside the material, due to the good mobility of the polymer chains at RT. In the case of 10ARA/90IL, the melting point of 1-ethyl-3-methylimidazolium bromide is observed around 75 °C, close to the value reported in the bibliography by Fredlake *et al.* [17] and also of the same order that the value measured in our previous works in which porous aramids were also obtained using this specific ionic liquid [37]. It is also interesting to remark that no plasticization effect of the ionic liquids in the aramid matrix was observed, indicating that the role of the aramid is exclusively acting as support of the mixing of ionic liquids, obtaining a material in which aramid and ionic liquid phases are completely separated, without any chemical interaction. On the other hand, we could not observe any thermal transition associated to the ARA_{IMID} film (composed of commercial ionic liquid EMIM TFSI and lithium salt LiTFSI together with polymerizable ionic liquid ILQ). Although we did expect to observe a similar transition to the one observed in in $ARA_{ILQ\text{-}pol}$ film, it may be due to the low proportion of ILQ employed in the polymerizable solution (around 24 %, see Table 1), and this transition could not be detected.

SEM observations of filled and polymerized aramids before and after washing with DCM were carried out to visually detect the presence of the polymerized ionic liquid ILQ, and the removal of the monomer with DCM. For comparison purposes, the SEM images of the initial porous aramid 10ARA/90IL-R, are included.

Fig. 2 presents the SEM images of the cross section and surface of the starting porous aramid (10ARA/90IL)-R), the filled aramid ($ARA_{ILQ\text{-}fil}$) and the polymerized aramid ($ARA_{ILQ\text{-}pol}$). Fig. 2a and d show the porous morphology of the starting porous aramid, and after filling with the polymerizable ionic liquid ILQ after the immersion in the polymerizable solution, Fig. 2b and e of the $ARA_{ILQ\text{-}fil}$ aramid. In the cross section and surface image, it is detected that the filling process is completed along the whole porous morphology. However, when polymerization occurs, the morphology observed changes drastically. In the cross-section image of $ARA_{ILQ\text{-}pol}$, Fig. 2c, the porous structure disappears, emerging a dense surface in which the polymerized ILQ is located in sub-micron regions. This region, distributed homogeneously, could correspond to fragments of aramid covered by the polymerized ILQ. On the contrary, surface morphology of the polymerized aramid, Fig. 2f of the $ARA_{ILQ\text{-}pol}$, does not differ greatly from the morphology observed in the filled aramid, Fig. 2e, and a dense surface morphology is detected. The difference between the cross-section and surface images in $ARA_{ILQ\text{-}pol}$ aramid could be explained as follows, in the case of surface observations, there is a thin layer of IL polymerized homogeneously, Fig. 2f, but in the inner porosity, it could be observe that the pores have been completely filled with the IL, Fig. 2c.

The effect of the washing process with DCM is presented in the SEM

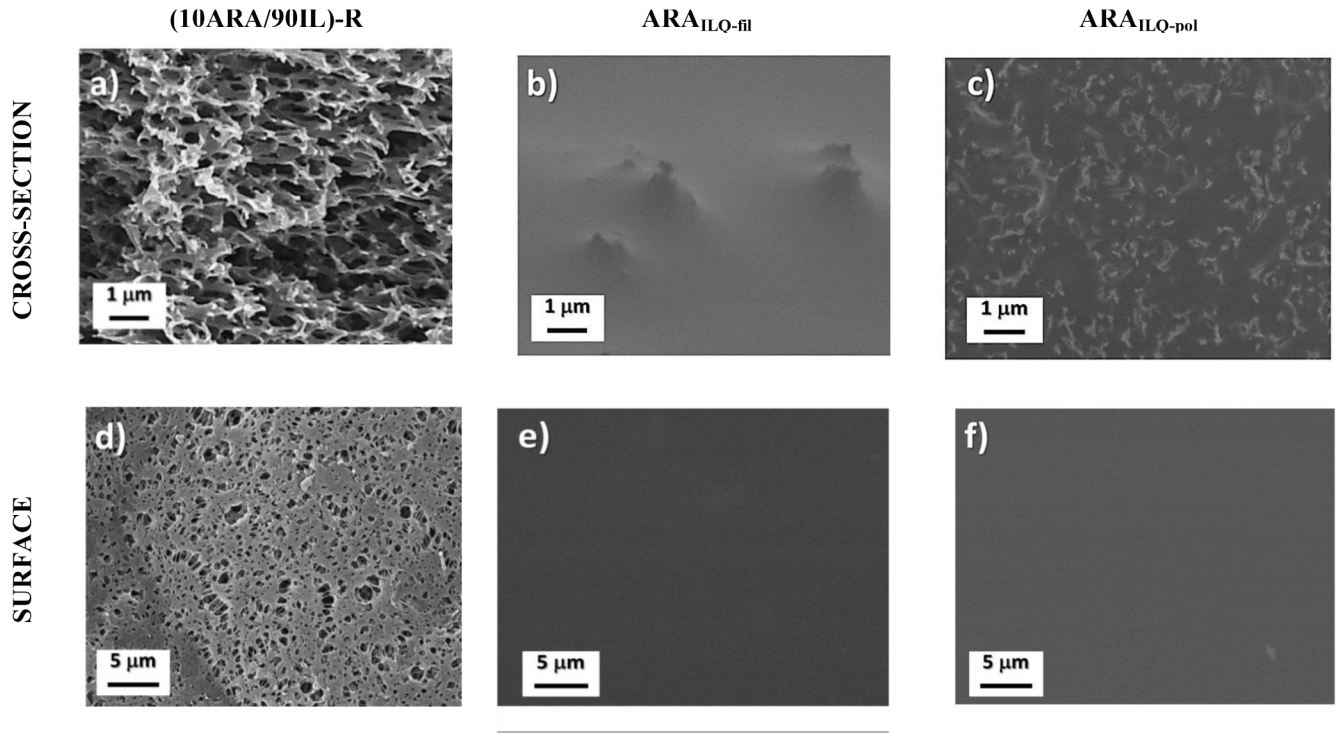

Fig. 2. SEM micrographs of the aramids: a) cross section of 10ARA/90IL-R; b) cross section of $ARA_{ILQ\text{-}fil}$; c) cross section of $ARA_{ILQ\text{-}pol}$; d) surface of (0ARA/90IL-R; e) surface of $ARA_{ILQ\text{-}fil}$; and f) Surface of $ARA_{ILQ\text{-}pol}$.

images in Fig. 3. Fig. 3a presents the surface of the filled aramid $ARA_{ILQ\text{-}fil}$ after washing with DCM, in which the porosity surface is revealed again due to the removal of the ILQ monomer. On the other hand, Fig. 3b shows that washing with DCM does not affect the polymerized membrane $ARA_{ILQ\text{-}pol}$ (no porosity appears, and dense surface is observed in the same way that in the filled aramid, see Fig. 2f). These results would confirm that photopolymerization of the ILQ monomer takes place inside the porous structure of the aramids.

Weight measurements were carried out to analyze two different phenomena. First, the filling ability of porous aramids is analyzed, which can be compared as an estimative process to the swelling percentage in dense aramids. The second phenomenon is intended to study the efficiency of the photopolymerization of the ILQ inside the porous structure. This can be evidenced simply by measuring the weight variation of a filled and a polymerized sample before and after washing with DCM. Due to the high solubility in DCM of the ILQ monomer and the insolubility of the polymerized ILQ, the polymerization process can be characterized.

Beginning with the filling behavior, Table 4 presents the weight variation of a porous aramid disc (ARA_{IMID}) before and after the filling process described in Section 3.2. Data presented in Table 4 results in a filling percentage of around 465 %. This value is considerably higher than filling percentages observed in dense aramids, which hardly exceed values around 10 % in aqueous solutions [38]. This data confirms the positive influence of the surface porosity in the filling ability of aramids, enhancing drastically the quantity of photopolymerizable formulation, and for instance the content of ionic-liquids (ILQ and EMIM TFSI) and Lithium salt, which could be embedded in the aramid porous structure.

Secondly, the efficiency of the polymerization process is simply analyzed by measuring the quantity of unreacted ILQ monomer that is eliminated through washing the material in DCM. For this purpose, masses of $ARA_{ILQ\text{-}pol}$ and $ARA_{ILQ\text{-}fil}$ discs were measured before and after washing with DCM. Results showed that mass loss percentage in $ARA_{ILQ\text{-}fil}$ was around 77 % in relation with the total weight of ARAILQ-fil disc, which corresponds to the ILQ monomer, and recovering fully the initial mass. On the other hand, mass loss percentage in $ARA_{ILQ\text{-}pol}$ was practically negligible (around 1.5 %), indicating the absence of unreacted monomer after the polymerization process.

3.3. Ionic conductivity

The values of conductivity (σ) at 25 °C in all the aramids prepared are listed in Table 5, and it was determined at the value of frequency where a maximum in tan δ graph was observed. Fig. S3 shows the conductivity and tan δ variation in the frequency range.

The analysis of the results can be categorized in three groups, in terms of their conductivity values. In the first group, it could be compared the starting porous aramid, 10ARA/90IL-R, with a practically negligible ionic conductivity, together with the aramid with the commercial ionic liquid embedded, 10ARA/90IL, with a high conductivity value of 1.19×10^{-3} S/cm, owing to the ionic liquid phase distributed in the aramid matrix, which was observed through RAMAN mapping tests in our previous works [25]. Despite this good value, in these materials the liquid phase could migrate out of the membrane as time goes by. Also, the total amount of commercial ionic liquid in each membrane disc is too high, around 225 mg/disc.

Secondly, it is therefore important to stand out the ionic conductivity values of only filled material ($ARA_{ILQ\text{-}fil}$) along with the aramid filled with the ionic liquid ILQ and polymerized ($ARA_{ILQ\text{-}pol}$). While the ionic conductivity of filled membrane ($ARA_{ILQ\text{-}fil}$) is in the range of the liquid electrolytes (0.244×10^{-3} S/cm), in the case of the polymerized aramid ($ARA_{ILQ\text{-}pol}$) the value drops down to 0.35×10^{-6} S/cm. This result would be due to the fact that in the case of $ARA_{ILQ\text{-}pol}$, the IL is anchored to the polymer matrix and the ionic mobility would be drastically hindered and as consequence, the ionic conductivity decreases [21] (see Fig. S4a of the ESI).

Lastly, it must be stressed the ionic conductivity value of the porous aramid containing the polymerizable solution (ionic liquid ILQ and EMIM TFSI, and LiTFSI) and UV irradiated, ARA_{IMID}. This is an interesting strategy in the preparation of IL-based electrolytes, in order to increase the solid electrolyte conductivity [15]. In this case, the presence of ILQ is of great importance, not only because of their well-known advantages as far as security risks, but also due to the good chemical

Table 4
Filling percentage of porous aramid discs after the experimental procedure described in Section 3.2. (Discs immersed into photocurable solution and UV irradiated at 365 nm).

Initial mass (mg)	Final mass (mg)	ILQ (mg)	EMIM TFSI (mg)	LiTFSI (mg)	Filling (%)
20	113	23	51	19	465

Table 5
Conductivity values obtained in aramids at 25 °C.

Film	σ (S/cm)
10ARA/90IL	1.19×10^{-3}
10ARA/90IL-R	7.37×10^{-8}
ARA_{IMID}	1.23×10^{-3}
$ARA_{ILQ\text{-}fil}$	0.24×10^{-3}
$ARA_{ILQ\text{-}pol}$	0.35×10^{-6}

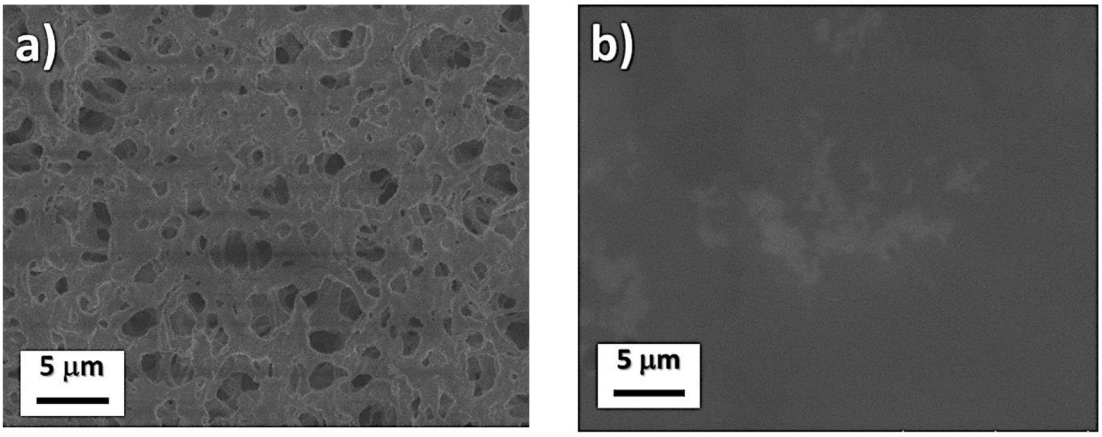

Fig. 3. SEM micrographs of the surface aramids after washing with DCM. a)$ARA_{ILQ\text{-}fil}$; b)$ARA_{ILQ\text{-}pol}$.

compatibility with the IL (EMIM TFSI) forming stable ion-gels with high conductivity values [20]. In this instance, a remarkable ionic conductivity of up to 1.23×10^{-3} S/cm at 25 °C is obtained, very closely to their analogous aramid with ionic liquid (10ARA/90IL). Furthermore, this value is in the range of the liquid electrolytes, such as the conductivity at 25 °C of liquids like EMIFSI (15.4×10^{-3} S/cm) [23], EMIMTFSI used in this work (5.3×10^{-3} S/cm) and for electrolytes based on EMIMTFSI and LiTFSI (values around 2.6–3.7 10^{-3} S/cm depending on the composition) [39]. In addition to this, the quantity of commercial IL in ARA_{IMID} is considerably lower (around 70 mg).

By comparing the ionic conductivity of the starting 10ARA/90IL and ARA_{IMID} aramids, the obtained values are similar, even slightly higher in ARA_{IMID} aramid. At this point, it is important to remark that the quantity of liquid IL (1-ethyl-3-methylimidazolium bromide) in 10ARA/90IL disc is around 225 mg (90% of the total weight), whereas this quantity in ARA_{IMID} is considerably lower, around 70 mg (65% of the total weight). Also, it must pointed out that in in ARA_{IMID} only 51 mg (45% of total weight) correspond to EMIMTFSI which remained as liquid phase in the membrane, since ILQ is photopolymerized. Moreover, in the case of 10ARA/90IL, the conductivity at 25 °C of pure 1-ethyl-3-methylimidazolium bromide is around 0.68×10^{-3} S/cm [40], whereas in the case of TFSI-based ionic liquids, this value is higher (between 3 and 10×10^{-3} S/cm) [41]. This indicates that the process of filling and "in situ" photopolymerization through the interconnected microchannel porous structure can reduce drastically the amount of commercial ionic liquid necessary to obtain high-conductive materials, and for instance would contribute to develop safer systems.

Thermal dependence of the ionic conductivity of ARA_{IMID} was also analyzed, indicating a temperature dependence characteristic of a viscous liquid in which ionic conductivity is governed by viscosity (μ) of the system in the whole temperature range. Fig. S5 of the ESI shows the evolution of the ionic conductivity of ARA_{IMID} between −50 °C and 90 °C, where the conductivity increased with temperature up to values around 10^{-2} S/cm.

4. Conclusions

This work presents a novel route to obtain flexible solid-gel polymer electrolytes based on porous aramids, and by using photopolymerization of ionic liquids to fill the porous structure. The membranes prepared combine the excellent thermal and mechanical properties of the aramids with high ionic conductivity values of ionic liquids. The determination of the ionic conductivity confirmed that values lied in the range of current solid-gel polymeric electrolytes reported in the literature. Also, the results would indicate that ion mobility is not only due to the intrinsic conductivity of the ionic liquid, but it is also enhanced by the interconnected porosity of the aramid, then increasing easily their efficiency as ion-conducting materials, suggesting a relation between the porous structure of the aramid and the ionic conductivity of the membrane. In addition, compared to other solid-gel polymer electrolytes, our method involves lower quantities of IL to obtain high ionic conductivity values, then improving the efficiency and safety of the polyelectrolytes employed in high-performance Li-ion batteries.

CRediT authorship contribution statement

M. Trigo López: Methodology, Investigation. **J.A. Reglero Ruiz:** Conceptualization, Supervision, Visualization, Writing – review & editing. **J.L. Pablos:** Methodology, Investigation, Visualization, Writing – review & editing. **D.E. Ciurduc:** Investigation. **T. Corrales:** Conceptualization, Supervision, Visualization, Writing – review & editing, Funding acquisition. **F.C. García:** Conceptualization, Visualization, Writing – review & editing, Writing – review & editing. **J.M. García:** Conceptualization, Supervision, Writing – review & editing, Funding acquisition.

Declaration of Competing Interest

The authors declare that they have no known competing financial interests or personal relationships that could have appeared to influence the work reported in this paper.

Acknowledgments

We gratefully acknowledge the financial support provided by FEDER (Fondo Europeo de Desarrollo Regional) and both the Spanish Ministerio de Economía, Industria y Competitividad (MAT2017-84501-R and MAT2017-88923-P), the Consejería de Educación-Junta de Castilla y León (BU306P18) and the Spanish Ministerio de Ciencia e Innovación (PID2019-108583RJ-I00/AEI/10.13039/501100011033).

Appendix A. Supplementary data

Supplementary data to this article can be found online at https://doi.org/10.1016/j.jphotochem.2021.113571.

References

[1] I. Osada, H. deVries, B. Scrosati, S. Passerini, Ionic-Liquid-Based Polymer Electrolytes for Battery Applications, Angew. Chemie - Int. Ed. 55 (2) (2016) 500–513, https://doi.org/10.1002/anie.201504971.
[2] D. Mecerreyes, L. Porcarelli, N. Casado, Innovative Polymers for Next-Generation Batteries, Macromol. Chem. Phys. 221 (4) (2020) 1900490, https://doi.org/10.1002/macp.201900490.
[3] N.K. Karan, D.K. Pradhan, R. Thomas, B. Natesan, R.S. Katiyar, Solid polymer electrolytes based on polyethylene oxide and lithium trifluoro- methane sulfonate (PEO–LiCF3SO3): Ionic conductivity and dielectric relaxation, 179 (2008) 689–696. doi:10.1016/j.ssi.2008.04.034.
[4] B.W. Zewde, S. Admassie, J. Zimmermann, S. Isfort, Enhanced Lithium Battery with Polyethylene Oxide-Based Electrolyte Containing Silane – Al2O3 Ceramic Filler, 3 (2013) 1–7. doi:10.1002/cssc.201300296.
[5] D. Zhou, X. Mei, J. Ouyang, Ionic Conductivity Enhancement of Polyethylene Oxide-$LiClO_4$ Electrolyte by Adding Functionalized Multi-Walled, Carbon Nanotubes 115 (33) (2011) 16688–16694, https://doi.org/10.1021/jp203224b.
[6] H. Yoon, G.H. Lane, Y. Shekibi, P.C. Howlett, M. Forsyth, A.S. Best, D. R. MacFarlane, Lithium electrochemistry and cycling behaviour of ionic liquids using cyano based anions, Energy Environ. Sci. 6 (2013) 979–986, https://doi.org/10.1039/c3ee23753b.
[7] S. Menne, J. Pires, M. Anouti, A. Balducci, Protic ionic liquids as electrolytes for lithium-ion batteries, Electrochem. Commun. 31 (2013) 39–41, https://doi.org/10.1016/j.elecom.2013.02.026.
[8] M.J. Park, I. Choi, J. Hong, O. Kim, Polymer electrolytes integrated with ionic liquids for future electrochemical devices, J. Appl. Polym. Sci. 129 (5) (2013) 2363–2376, https://doi.org/10.1002/app.39064.
[9] A. Vallée, S. Besner, J. Prud'Homme, Comparative study of poly(ethylene oxide) electrolytes made with $LiN(CF_3SO_2)_2$, $LiCF_3SO_3$ and $LiClO_4$: Thermal properties and conductivity behaviour, Electrochim. Acta. 37 (1992) 1579–1583, https://doi.org/10.1016/0013-4686(92)80115-3.
[10] A. Tsurumaki, J. Kagimoto, H. Ohno, Properties of polymer electrolytes composed of poly(ethylene oxide) and ionic liquids according to hard and soft acids and bases theory, Polym. Adv. Technol. 22 (2011) 1223–1228, https://doi.org/10.1002/pat.1931.
[11] S.K. Chaurasia, R.K. Singh, S. Chandra, Ion-polymer and ion-ion interaction in PEO-based polymer electrolytes having complexing salt $LiClO_4$ and/or ionic liquid, [BMIM][PF_6], J. Raman Spectrosc. 42 (12) (2011) 2168–2172, https://doi.org/10.1002/jrs.v42.1210.1002/jrs.2999.
[12] Z. Xue, D. He, X. Xie, Poly(ethylene oxide)-based electrolytes for lithium-ion batteries, J. Mater. Chem. A. 3 (38) (2015) 19218–19253, https://doi.org/10.1039/C5TA03471J.
[13] M.Z. Kufian, M.F. Aziz, M.F. Shukur, A.S. Rahim, N.E. Ariffin, N.E.A. Shuhaimi, S. R. Majid, R. Yahya, A.K. Arof, PMMA-LiBOB gel electrolyte for application in lithium ion batteries, Solid State Ionics 208 (2012) 36–42, https://doi.org/10.1016/j.ssi.2011.11.032.
[14] R.C. Agrawal, G.P. Pandey, Solid polymer electrolytes: Materials designing and all-solid-state battery applications: An overview, J. Phys. D. Appl. Phys. 41 (22) (2008) 223001, https://doi.org/10.1088/0022-3727/41/22/223001.
[15] J.L. Pablos, N. García, L. Garrido, F. Catalina, T. Corrales, P. Tiemblo, Polycationic scaffolds for Li-ion anion exchange transport in ion gel polyelectrolytes, J. Mater. Chem. A. 6 (24) (2018) 11215–11225, https://doi.org/10.1039/C8TA03134G.
[16] M. Egashira, H. Todo, N. Yoshimoto, M. Morita, J.-I. Yamaki, Functionalized imidazolium ionic liquids as electrolyte components of lithium batteries, J. Power Sources. 174 (2) (2007) 560–564, https://doi.org/10.1016/j.jpowsour.2007.06.123.

[17] C.P. Fredlake, J.M. Crosthwaite, D.G. Hert, S.N.V.K. Aki, J.F. Brennecke, Thermophysical properties of imidazolium-based ionic liquids, J. Chem. Eng. Data. 49 (4) (2004) 954–964, https://doi.org/10.1021/je034261a.
[18] H.L. Ngo, K. LeCompte, L. Hargens, A.B. McEwen, Thermal properties of imidazolium ionic liquids, Thermochim. Acta. 357–358 (2000) 97–102, https://doi.org/10.1016/S0040-6031(00)00373-7.
[19] M.D. Green, T.E. Long, Designing imidazole-based ionic liquids and ionic liquid monomers for emerging technologies, Polym. Rev. 49 (4) (2009) 291–314, https://doi.org/10.1080/15583720903288914.
[20] A.S. Shaplov, R. Marcilla, D. Mecerreyes, Recent Advances in Innovative Polymer Electrolytes based on Poly(ionic liquid)s, Electrochim. Acta. 175 (2015) 18–34, https://doi.org/10.1016/j.electacta.2015.03.038.
[21] S. Washiro, M. Yoshizawa, H. Nakajima, H. Ohno, Highly ion conductive flexible films composed of network polymers based on polymerizable ionic liquids, Polymer (Guildf). 45 (5) (2004) 1577–1582, https://doi.org/10.1016/j.polymer.2004.01.003.
[22] Y. Aihara, M. Kodama, K. Nakahara, H. Okise, K. Murata, Characteristics of a thin film lithium-ion battery using plasticized solid polymer electrolyte, J. Power Sources. 65 (1-2) (1997) 143–147, https://doi.org/10.1016/S0378-7753(96)02605-5.
[23] G.B. Appetecchi, G.-T. Kim, M. Montanino, M. Carewska, R. Marcilla, D. Mecerreyes, I. De Meatza, Ternary polymer electrolytes containing pyrrolidinium-based polymeric ionic liquids for lithium batteries, J. Power Sources. 195 (11) (2010) 3668–3675, https://doi.org/10.1016/j.jpowsour.2009.11.146.
[24] J.L. Pablos, N. García, L. Garrido, J. Guzmán, F. Catalina, T. Corrales, P. Tiemblo, Highly efficient mixed Li^+ transport in ion gel polycationic electrolytes, J. Memb. Sci. 545 (2018) 133–139, https://doi.org/10.1016/j.memsci.2017.08.073.
[25] B.S. Pascual, M. Trigo-López, J.A. Reglero Ruiz, J.L. Pablos, J.C. Bertolín, C. Represa, J.V. Cuevas, F.C. García, J.M. García, Porous aromatic polyamides the easy and green way, Eur. Polym. J. 116 (2019) 91–98, https://doi.org/10.1016/j.eurpolymj.2019.03.058.
[26] H. Lin, S. Zhang, J.-K. Sun, M. Antonietti, J. Yuan, Poly (ionic liquid)s with engineered nanopores for energy and environmental applications, Polymer (Guildf). 202 (2020) 122640, https://doi.org/10.1016/j.polymer.2020.122640.
[27] J. Zhang, B. Sun, X. Huang, S. Chen, G. Wang, Honeycomb-like porous gel polymer electrolyte membrane for lithium ion batteries with enhanced safety, Sci. Rep. 4 (2014) 1–7, https://doi.org/10.1038/srep06007.
[28] R. Miao, B. Liu, Z. Zhu, Y. Liu, J. Li, X. Wang, Q. Li, PVDF-HFP-based porous polymer electrolyte membranes for lithium-ion batteries, J. Power Sources 184 (2) (2008) 420–426, https://doi.org/10.1016/j.jpowsour.2008.03.045.
[29] R. Rohan, Y. Sun, W. Cai, K. Pareek, Y. Zhang, G. Xu, H. Cheng, Functionalized meso/macro-porous single ion polymeric electrolyte for applications in lithium ion batteries, J. Mater. Chem. A. 2 (9) (2014) 2960–2967, https://doi.org/10.1039/C3TA13765A.
[30] D. Zhou, R. Liu, J. Zhang, X. Qi, Y.-B. He, B. Li, Q.-H. Yang, Y.-S. Hu, F. Kang, Nano Energy In situ synthesis of hierarchical poly(ionic liquid)-based solid electrolytes for high-safety lithium-ion and sodium-ion batteries, Nano Energy 33 (2017) 45–54, https://doi.org/10.1016/j.nanoen.2017.01.027.
[31] L. Oliveira-Salmazo, A. Lopez-Gil, F. Silva-Bellucci, A.E. Job, M.A. Rodriguez-Perez, Natural rubber foams with anisotropic cellular structures: Mechanical properties and modeling, Ind. Crops Prod. 80 (2016) 26–35, https://doi.org/10.1016/j.indcrop.2015.10.050.
[32] J.A.R. Ruiz, S. Vallejos, B.S. Pascual, C. Ramos, S. Beltrán, F.C. García, J.M. García, Microcellular polymer films based on cross-linked 1-vinyl-2-pyrrolidone and methyl methacrylate, J. Supercrit. Fluids. 140 (2018) 270–278, https://doi.org/10.1016/j.supflu.2018.07.011.
[33] D. Santos, M. Santos, E. Franceschi, C. Dariva, A. Barison, S. Mattedi, Experimental Density of Ionic Liquids and Thermodynamic Modeling with Group Contribution Equation of State Based on the Lattice Fluid Theory, J. Chem. Eng. Data. 61 (1) (2016) 348–353, https://doi.org/10.1021/acs.jced.5b00592.
[34] R.L. Gardas, M.G. Freire, P.J. Carvalho, I.M. Marrucho, I.M.A. Fonseca, A.G. M. Ferreira, J.A.P. Coutinho, High-pressure densities and derived thermodynamic properties of imidazolium-based ionic liquids, J. Chem. Eng. Data. 52 (1) (2007) 80–88, https://doi.org/10.1021/je060247x.
[35] M. Trigo-López, S. Vallejos, J.A. Reglero Ruiz, C. Ramos, S. Beltrán, F.C. García, J. M. García, Fabrication of microporous PMMA using ionic liquids: An improved route to classical $ScCO_2$ foaming process, Polymer (Guildf). 183 (2019) 121867, https://doi.org/10.1016/j.polymer.2019.121867.
[36] Y. Cao, T. Mu, Comprehensive investigation on the thermal stability of 66 ionic liquids by thermogravimetric analysis, Ind. Eng. Chem. Res. 53 (20) (2014) 8651–8664, https://doi.org/10.1021/ie5009597.
[37] M. Trigo-López, S. Vallejos, J.A. Reglero Ruiz, A. García-Gómez, M. Seara-Martínez, F.C. García, J.M. García, High-performance nanoporous aramid films reinforced with functionalized carbon nanocharges using ionic liquids, Polymer (Guildf). 202 (2020) 122629, https://doi.org/10.1016/j.polymer.2020.122629.
[38] J.A. Reglero Ruiz, M. Trigo-López, F.C. García, J.M. García, Functional aromatic polyamides, Polymers (Basel) 9 (2017), https://doi.org/10.3390/polym9090414.
[39] M. Kerner, N. Plylahan, J. Scheers, P. Johansson, Ionic liquid based lithium battery electrolytes:fundamental benefits of utilising both TFSI and FSI anions? Phys. Chem.Chem.Phys.,17 (2015) 19569–1958. doi: 10.1039/c5cp01891a.
[40] J. Vila, C. Franjo, J.M. Pico, L.M. Varela, O. Cabeza, Temperature Behavior of the Electrical Conductivity of Emim-Based Ionic Liquids in Liquid and Solid States, Portugaliae, Electrochimica Acta 25 (1) (2007) 163–172.
[41] Y. Fu, X. Cui, Y. Zhang, T. Feng, J. He, X. Zhang, X. Bai, Q. Cheng, Measurement and Correlation of the Electrical Conductivity of the Ionic Liquid [BMIM][TFSI] in Binary Organic Solvents, J. Chem. Eng. Data. 63 (5) (2018) 1180–1189, https://doi.org/10.1021/acs.jced.7b00646.